Available online at www.sciencedirect.com
ScienceDirect
Advances in Space Research 45 (2010) 99–111
ADVANCES IN SPACE RESEARCH (a COSPAR publication)
www.elsevier.com/locate/asr

Local luminous infrared galaxies: Spatially resolved mid-infrared observations with *Spitzer*/IRS ☆

Almudena Alonso-Herrero [a,b,*], Miguel Pereira-Santaella [a], George H. Rieke [b], Luis Colina [a], Charles W. Engelbracht [b], Pablo G. Pérez-González [b,c], Tanio Díaz-Santos [a,1], J.-D.T. Smith [d]

[a] *Instituto de Estructura de la Materia, CSIC, Serrano 121, E-28006, Madrid, Spain*
[b] *Steward Observatory, University of Arizona, 933 N. Cherry Avenue, Tucson, AZ 85721, USA*
[c] *Departamento de Astrofísica, Facultad de CC. Físicas, Universidad Complutense de Madrid, Avenida Complutense S/N, E-28040, Madrid, Spain*
[d] *Ritter Astrophysical Research Center, University of Toledo, 2801 West Bancroft Street, Toledo, OH 43603, USA*

Received 15 April 2009; received in revised form 11 August 2009; accepted 11 August 2009

Abstract

Luminous Infrared (IR) Galaxies (LIRGs, $L_{IR} = 10^{11}$–10^{12} $L_{\odot}$) are an important cosmological class of galaxies as they are the main contributors to the co-moving star formation rate density of the universe at $z = 1$. In this paper we present a guaranteed time observation (GTO) *Spitzer* InfraRed Spectrograph (IRS) program aimed to obtain spectral mapping of a sample of 14 local ($d < 76$ Mpc) LIRGs. The data cubes map, at least, the central 20 arcsec × 20 arcsec to 30 arcsec × 30 arcsec regions of the galaxies, and use all four IRS modules covering the full 5–38 μm spectral range. The final goal of this project is to characterize fully the mid-IR properties of local LIRGs as a first step to understanding their more distant counterparts. In this paper we present the first results of this GTO program. The IRS spectral mapping data allow us to build spectral maps of the bright mid-IR emission lines (e.g., [Ne II]12.81 μm, [Ne III]15.56 μm, [S III]18.71 μm,H_2 at 17 μm), continuum, the 6.2 and 11.3 μm polycyclic aromatic hydrocarbon (PAH) features, and the 9.7 μm silicate feature, as well as to extract 1D spectra for regions of interest in each galaxy. The IRS data are used to obtain spatially resolved measurements of the extinction using the 9.7 μm silicate feature, and to trace star forming regions using the neon lines and the PAH features. We also investigate a number of active galactic nuclei (AGN) indicators, including the presence of high excitation emission lines and a strong dust continuum emission at around 6 μm. We finally use the integrated *Spitzer*/IRS spectra as templates of local LIRGs. We discuss several possible uses for these templates, including the calibration of the star formation rate of IR-bright galaxies at high redshift. We also predict the intensities of the brightest mid-IR emission lines for LIRGs as a function of redshift, and compare them with the expected sensitivities of future space IR missions.

Keywords: Galaxies: evolution; Galaxies: nuclei; Galaxies: Seyfert; Galaxies: structure; Infrared: galaxies

1. Introduction

The importance of infrared (IR) bright galaxies has been increasingly appreciated since their discovery more than 30 years ago (Rieke and Low, 1972), and the detection of large numbers by *IRAS* (Soifer et al., 1987). Although the Ultraluminous Infrared Galaxies (ULIRGs, *with IR luminosities* 8–1000 μm,$L_{IR} = 10^{12}$–10^{13} $L_{\odot}$) get much of the attention because they are so dramatic, Luminous Infrared Galaxies (LIRGs, $L_{IR} = 10^{11}$–10^{12} $L_{\odot}$) are much more common,

☆ Based on observations obtained with the *Spitzer* Space Telescope, which is operated by the Jet Propulsion Laboratory, California Institute of Technology, under NASA Contract 1407.

* Corresponding author. Address: Instituto de Estructura de la Materia, CSIC, Serrano 121, E-28006, Madrid, Spain. Tel.: +34 91 5616800.
E-mail address: aalonso@damir.iem.csic.es (A. Alonso-Herrero).
[1] Present address: University of Crete, Department of Physics, P.O. Box 2208, GR-71003, Heraklion, Greece.

0273-1177/$36.00 © 2009 COSPAR. Published by Elsevier Ltd. All rights reserved.
doi:10.1016/j.asr.2009.08.010

accounting for $\sim 5\%$ of the local IR background compared with <1% for the ULIRGs (Lagache et al., 2005). They are of intrinsic interest because they provide insight to star formation and nuclear activity under extreme conditions and should also include former ULIRGs where the star formation is dying off (see Murphy et al., 2001). They take part in the controversy over the formation of AGN and its relation to star formation and high levels of IR emission (see review by Sanders and Mirabel, 1996).

Local LIRGs may also be prototypes for forming galaxies at high redshift (Lagache et al., 2005). Deep *Spitzer* detections at 24 μm are dominated by LIRGs and ULIRGs. LIRGs are the main contributors to the co-moving star formation rate (SFR) density in the $z \sim 1$–2 range (Elbaz et al., 2002; Le Floc'h et al., 2005; Pérez-González et al., 2005; Caputi et al., 2007), and contribute nearly 50% of the cosmic IR background at $z \sim 1$ (Lagache et al., 2005). Moreover, the mid-IR spectra of high redshift ($z \sim 2$) very luminous IR galaxies ($L_{IR} > 10^{12} L_{\odot}$) are more similar to those of local starbursts and LIRGs (see e.g., Farrah et al., 2008; Rigby et al., 2008; Alonso-Herrero et al., 2009) than those of local ULIRGs. This may just reflect the fact that at high-z star-formation was taking place over a few kiloparsec scales rather than in very compact (<1 kpc) regions as is the case for local ULIRGs (e.g., Soifer et al., 2000).

Much of our knowledge of the mid-IR spectroscopic properties of local IR-bright galaxies comes from *ISO* (e.g., Genzel et al., 1998; Rigopoulou et al., 1999; Tran et al., 2001) and early results (Armus et al., 2004, 2007) with the InfraRed Spectrograph (IRS, Houck et al., 2004) on *Spitzer*. However, the majority of the *ISO* works focused on samples of local IR-bright galaxies or starburst galaxies, and only include a few luminous LIRGs ($\log L_{IR} \simeq 11.80$ $L_{\odot}$, see e.g., Genzel et al., 1998; Verma et al., 2003). The majority of the recent *Spitzer* results are concentrating on ULIRGs (e.g., Armus et al., 2007; Farrah et al., 2007), starburst galaxies (Brandl et al., 2006), and nearby star-forming galaxies (Dale et al., 2006; Smith et al., 2007a). *Recently,* Armus et al. (2009) *have presented the Great Observatories All-Sky LIRG Survey (GOALS) project which combines multiwavelength data, including Spitzer, of over 200 low-redshift* ($z < 0.088$) *LIRGs.*

In this paper we summarize the goals and present the first results of a *Spitzer*/IRS program intended to obtain mid-IR (5–38 μm) spectral mapping of a representative sample of fourteen local LIRGs (Table 1) selected from the volume-limited sample of Alonso-Herrero et al. (2006a). It is only by quantifying the integrated spectroscopic properties of a representative sample of local LIRGs that we can interpret measurements at $z \sim 1$, which apply to the integrated galaxy. The final goal of this project is to characterize fully the mid-IR properties of local LIRGs as a first step to understanding their more distant counterparts. The complete results from this LIRG program will be presented in a number of forthcoming papers (Pereira-Santaella et al., 2009a,b in preparation). The paper is organized as follows. Section 2 presents the sample, observations and data reduction. Section 3 characterizes the obscuration of LIRGs and Section 4 discusses

Table 1
The sample of local LIRGs mapped with the IRS.

Galaxy name	IRAS name	v_{hel} (km s^{-1})	Dist (Mpc)	$\log L_{IR}$ ($L_{\odot}$)	Spect. class
(1)	(2)	(3)	(4)	(5)	(6)
NGC 2369	IRASF 07160-6215	3237	44.0	11.10	–
NGC 3110	IRASF 10015-0614	5034	73.5	11.31:	H II
NGC 3256*	IRASF 10257-4339	2814	35.4	11.56	H II
Arp 299**	IRASF 11257+5850	3121	47.7	11.88	H II, Sy2
ESO 320-G030	IRASF 11506-3851	3232	37.7	11.10	H II
NGC 5135	IRASF 13229-2934	4112	52.2	11.17	Sy2
Zw 049.057	IRASF 15107+0724	3897	59.1	11.27:	H II
–	IRASF 17138-1017	5197	75.8	11.42	H II
IC 4687/IC 4686***	IRASF 18093-5744	5200/4948	74.1	11.55:	H II (both)
NGC 6701	IRASF 18425+6036	3965	56.6	11.05	Composite
NGC 7130	IRASF 21453-3511	4842	66.0	11.35	Sy/L
IC 5179	IRASF 22132-3705	3422	46.7	11.16	H II
NGC 7591	IRASF 23157+0618	4956	65.5	11.05	Composite
NGC 7771	IRASF 23488+1949	4277	57.1	11.34	H II

Notes. Column (1): galaxy name. *NGC 3256 is a merger system with two nuclei, refered to as north and south. **Arp 299 is composed of IC 694 (eastern component) and NGC 3690 (western component). ***Only IC 4687 was observed in spectral mapping mode. Column (2): *IRAS* denomination from Sanders et al. (2003). Column (3): heliocentric velocity from NED. Column (4): distance taken from Sanders et al. (2003) assuming $H_0 = 75$ km s^{-1} Mpc^{-1}. Column (5): 8–1000 μm IR luminosity taken from Sanders et al. (2003), where the suffix ":" means large uncertainty (see Sanders et al., 2003 for details). *The IR luminosity is for the system Arp 299 = IC 694 + NGC 3690. Column (6): nuclear activity class from optical spectroscopy. "Sy" = Seyfert, "*Composite*" = *intermediate between LINER and H II (see* Alonso-Herrero et al., 2009b*)*, "H II" = H II region-like, "–" = no classification available. *The classifications for Arp 299 are: nuclear region of IC 694, or source A, is H II-like, and the nuclear region of NGC 3690, or source B1, is a Sy2. The references for the nuclear class are given by Alonso-Herrero et al. (2006a), except for the nuclear region of NGC 3690 which is from García-Marín et al. (2006), and NGC 6701 and NGC 7591, which are reported by Alonso-Herrero et al. (2009b).

the AGN and star formation properties of the sample. Section 5 presents the integrated mid-IR spectra and their potential use for studies of IR-bright galaxies at high-z. Finally Section 6 gives a summary of this work.

2. Sample, *Spitzer*/IRS spectral mapping observations, and data reduction

The galaxies chosen for this study are taken from a representative *and volume-limited* sample of LIRGs originally drawn from the *IRAS* Revised Bright Galaxy Sample (Sanders et al., 2003) for Paα imaging (using a narrow-band filter) with NICMOS on the *HST* (Alonso-Herrero et al., 2006a). Hence both the NICMOS sample and the sub-sample selected for IRS observations are restricted in redshift ($d < 76$ Mpc). *For this IRS program we chose LIRGs in this sample with extended Paα and mid-IR emission* (Alonso-Herrero et al., 2006a and Díaz-Santos et al., 2008a) *so we could map out most of the IR emission of these galaxies. This is important for comparison with IR-selected high-z galaxies where the entire galaxy is encompassed in the IRS slit.*

As can be seen from Table 1, the IRS sample covers well the range of IR luminosity of LIRGs (see Sanders et al., 2003), and the nuclear activity classes of LIRGs. *For this sample, $\sim 30\%$ are classified as AGN, if we include composite objects, that is, nuclei classified as intermediate between H II and LINER using optical line ratios (see* Alonso-Herrero et al., 2009b*). This fraction is similar to that found for LIRGs by* Veilleux et al. (1995). The IR luminosities of this sample imply SFRs of between 19 and 130 $M_\odot$ yr^{-1}, using the Kennicutt (1998) prescription. In Alonso-Herrero et al. (2009) we recently presented a detailed study of Arp 299.

We obtained IRS mapping observations of the LIRG sample using all four modules: Short-High (SH; 9.9–19.6 μm), Long-High (LH; 18.7–37.2 μm), Short-Low (SL1; 7.4–14.5 μm and SL2; 5.2–7.7 μm) and Long-Low (LL1; 19.5–38 μm and LL2; 14.0–21.3 μm). The plate scales are 1.85, 2.26, 4.46, and 5.08 arcsec per pixel for the SL, SH, LH, and LL modules, respectively. The IRS high spectral resolution data (SH and LH modules) have $R \sim 600$, whereas the low resolution spectra (SL and LL) have $R \sim 60$–126.

The majority of the observations were obtained in Cycle 3 and Cycle 4 as part of a *Spitzer* guaranteed time observation (GTO) program (P.I.: G.H. Rieke, programs ID 30577 and ID 40479), except for the low spectral resolution observations (SL and LL modules) of Arp 299, which were part of a different GTO program (P.I.: J.R. Houck, program ID 21) observed in Cycle 1.

We used the IRS spectral mapping capability, which involves moving the telescope perpendicular to the long axis of the slit with a step of one-half the slit width until the appropriate region is covered. Since in most cases the SL (*length of 57 arcsec*) and LL (*length of 168 arcsec*) slits are longer than the extent of the galaxies, we did not obtain separate background observations. For the LH module we obtained dedicated background observations in staring mode (one single slit) at a region about 2 arcmin away from the galaxy. We did not observe backgrounds for the SH module, *except for those galaxies observed in Cycle 4 (NGC 6701, NGC 7591, and NGC 7771)*. We mapped approximately at least the central 20 arcsec × 20 arcsec to 30 arcsec × 30 arcsec regions of the galaxies (before rotation). The sizes of the maps were chosen to cover a large fraction of the mid-IR emission of these galaxies. For the typical distances of our LIRGs, the IRS maps cover the central ~ 3–11 kpc, depending on the galaxy and the IRS module. Table 2 summarizes the *Spitzer*/IRS observing parameters used for our GTO program.

We processed the data using the *Spitzer* IRS pipeline version S15.3 for the SL and LL modules, and S17.2 for the SH and LH modules. The data cubes were assembled using CUBISM (the CUbe Builder for IRS Spectra Maps, Smith et al., 2007b) from the individual Basic Calibrated Data (BCD) spectral images. Full error cubes are also built alongside the data cubes by standard error propagation, using, for the input uncertainty, the BCD-level uncertainty estimates produced by the IRS pipeline from deviations of the fitted ramp slope fits for each pixel. These uncertainties are used to provide error estimates for the extracted spectra, and for the line and continuum maps (see Smith et al., 2007b for full details). The angular resolutions (FWHM) of the data cubes are ~ 4 arcsec, and ~ 5 arcsec for the SL and SH modules, respectively (see Pereira-Santaella et al., 2009a). For the distances of our galaxies, these correspond to physical scales of between ~ 0.7 kpc for the nearest objects to ~ 2 kpc for the most distant ones.

We extracted nuclear 1D spectra for all the IRS modules using CUBISM with the smallest (2 × 2 pixel) possible extraction apertures from the data cubes before rotation. We also extracted 1D low-resolution (SL + LL) spectra covering approximately the extent of each system to be representative of the mid-IR properties of the LIRGs (see Section 5).

Table 2
IRS observing parameters.

Module	Step Perp	Perp Points	Step Pars	Par Points	t (s)	Cycles
(1)	(2)	(3)	(4)	(5)	(6)	(7)
SL1	1.8	13 (17)	–	–	14	2
SL2	1.8	13 (17)	–	–	14	2
LL1	5.25	5 (7)	–	–	14	2
LL2	5.25	5 (7)	–	–	14	2
SH	2.35	9 (15)	5.65	5 (7)	30	2
LH	5.55	5 (7)	–	–	60	4

Notes. Column (1): IRS Module. Column (2): size of the step along the direction perpendicular to the slit in arcseconds. Column (3): number of steps in the perpendicular direction for the 20 arcsec × 20 arcsec maps, and for the 30 arcsec × 30 arcsec in brackets. Column (4): size of the step along the direction parallel to the slit in arcseconds. Column (5): number of steps in the parallel direction. Column (6): duration of the ramp in seconds. Column (7): number of cycles.

Full details on the observations, data reduction, and the construction of the data cubes, and spectral maps will be given by Pereira-Santaella et al. (2009a).

3. Characterizing the obscuration of LIRGs with the 9.7 m silicate feature

LIRGs, ULIRGs and IR-bright galaxies are known to contain highly obscured regions ($A_V \simeq 4-50$ mag, see e.g., Veilleux et al., 1995; Genzel et al., 1998; Alonso-Herrero et al., 2006a; Spoon et al., 2000, 2001; Roussel et al., 2006; Sirocky et al., 2008), and are usually coincident with the nucleus. In addition to the "traditional" values derived using hydrogen recombination lines (e.g., Hα/Hβ, *Pa*α/Hα), we can derive the distribution of the extinction using our spatially resolved maps of the depth of the 9.7 μm absorption feature. The apparent strength of the 9.7 μm silicate feature is defined as $S_{Si} = \ln f_{obs}(9.7\,\mu m)/f_{cont}(9.7\,\mu m)$, where $f_{cont}(9.7\,\mu m)$ is the local continuum and $f_{obs}(9.7\,\mu m)$ is the observed flux density of the feature. Negative values of the apparent strength of the feature mean that the feature is observed in absorption, whereas positive values mean that the feature is in emission. We used a method similar to that outlined by Spoon et al. (2007) for sources dominated by polycyclic aromatic hydrocarbon (PAH) emission, to fit the local continuum as a power law with pivot wavelengths at 5.5 and 14 μm. We extracted spectra with 2 pixel × 2 pixel apertures, by moving pixel by pixel along columns and rows until the entire field of view was covered. We built the spectral maps of the silicate feature by measuring it on the individual 1D spectra. Assuming an extinction law and a dust geometry the silicate strength can be converted into a visual extinction. For comparison we also constructed maps of the 5.5 μm continuum, that is, of the mean flux of a bandpass covering the spectral range of 5.3–5.7 μm.

Fig. 1 shows the spectral maps of the apparent strength of the 9.7 μm silicate feature for two systems in our sample with very different behaviors, together with the maps of the 5.5 μm continuum. Arp 299 is the most luminous system in our sample (Table 1). It is a pair interacting galaxies composed of IC 694 and NGC 3690, whose nuclear regions are refered to as source A and source B1, respectively. As can be seen from Fig. 1, this system shows a large range of values of the silicate feature. The region with the deepest silicate feature ($S_{Si} \sim -2.2$, see Alonso-Herrero et al., 2009 for more details) is Arp 299-A and has a value comparable to the typical values of ULIRGs (see Armus et al., 2007; Spoon et al., 2007, and also next section). The implied extinction for Arp 299-A is $A_V \sim 36$ mag for a foreground screen of dust (assuming $A_V/\tau_{Si} = 16.6$; Rieke and Lebofsky, 1985), in agreement with previous works (see e.g., Gallais et al., 2004; Alonso-Herrero et al., 2000). *We note, however, that the measured silicate strength offers only a lower limit to the true extinction (e.g.,* Levenson et al., 2007*;* Sirocky et al., 2008*).* For Arp 299-B1, we measured $S_{Si} \sim -0.8$, which is in the range observed for Seyfert 2

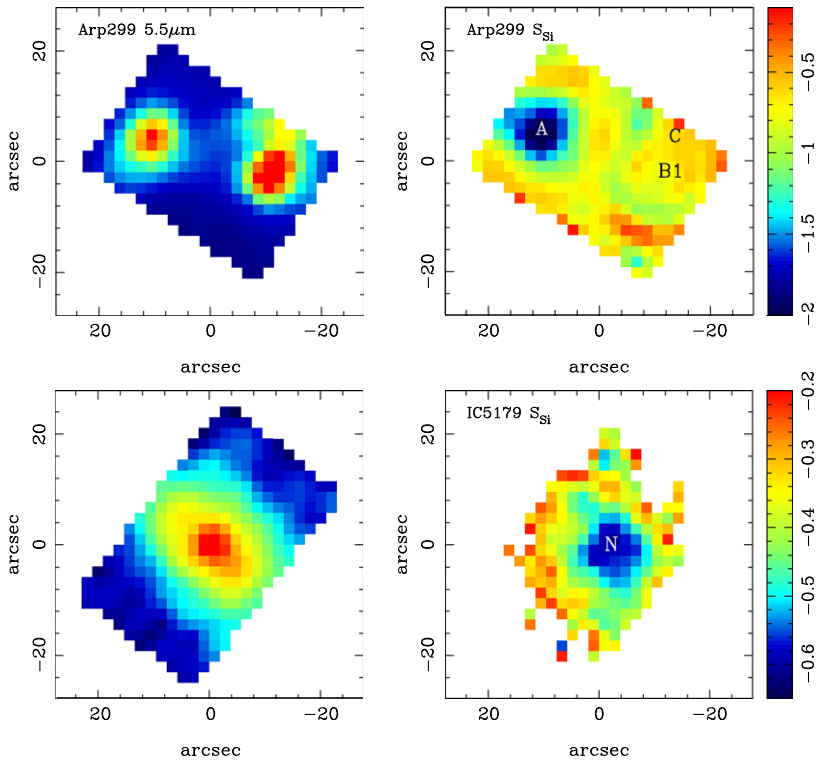

Fig. 1. IRS spectral maps of the continuum emission at 5.5 μm (left panels) and the apparent depth of the 9.7 μm silicate feature (right panels) of two LIRGs in our sample from the SL data cubes. For Arp 299 we mark the positions of the two nuclei: A for IC 694 (the eastern component) and B1 for NGC 3690 (the western component), as well as region C, an actively star forming region. For IC 5179 we mark the nuclear region as N. The maps have been rotated so the orientation is north up, east to the left.

galaxies (Shi et al., 2006; Hao et al., 2007). The values of the apparent depth of the silicate feature throughout the rest of this system are relatively moderate and similar to the values measured in other starburst galaxies (Brandl et al., 2006; Spoon et al., 2007).

The other galaxy shown in Fig. 1 is IC 5179, a spiral galaxy with a moderate IR luminosity (Table 1). The apparent depth of the silicate feature in the nuclear region is $S_{Si} \sim -0.5$, whereas in the circumnuclear regions the silicate feature is shallower indicating a lower extinction. This behavior is seen in a large fraction of the LIRGs in our sample (see Pereira-Santaella et al., 2009a).

The nuclear values of the apparent depth of the silicate feature for the galaxies in our sample can be seen in Fig. 2. For the distances of our galaxies the SL nuclear extraction apertures probe regions with physical sizes of between 0.6 and 1.4 kpc, depending on the galaxy. As can be seen from Fig. 2 the apparent depths of the silicate features of the majority of the LIRG nuclei are moderate ($S_{Si} \sim -0.4$ to -0.9), and intermediate between those observed in starburst galaxies (Brandl et al., 2006) and ULIRGs (Spoon et al., 2007). Using the Rieke and Lebofsky (1985) extinction law and assuming a foreground screen of dust, the observed apparent depths translate into typical nuclear extinctions of $A_V \sim 7$–15 mag. For the most obscured nuclei in our sample: Arp 299-A, the southern nucleus of NGC 3256, and Zw 049.057, the nuclear extinctions are in excess of $A_V \sim 20$ mag (assuming a foreground screen of dust).

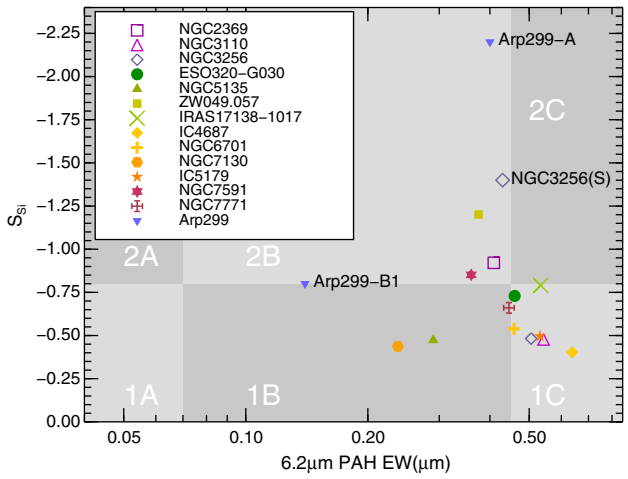

Fig. 2. Diagram of the EW of the 6.2 μm PAH feature versus the apparent depth of the 9.7 μm silicate feature for the nuclei of the galaxies in our sample. These quantities were measured from SL spectra extracted with 3.7 arcsec × 3.7 arcsec apertures *centered at the nuclei of the galaxies*. The different regions in this diagram are taken from Spoon et al. (2007). Region 1A is occupied by AGN and it is characterized by low EW of the PAH feature and a weak silicate feature. Region 1C has moderate silicate feature in absorption *to nearly-zero* and high EW of the PAH, and it is mostly occupied by starburst galaxies. Region 1B is intermediate between the previous two, and it is occupied by galaxies with both AGN and star formation. Most ULIRGs in the Spoon et al. (2007) sample fall in region 2B and region 3A. The 3A (very deep silicate feature and low EW of the 6.2 μm PAH feature), 3B and 3C regions of Spoon et al. (2007) are not shown in this figure.

4. The AGN and star formation properties of LIRGs

4.1. Identifying AGN in the mid-IR

Composite (AGN + starburst) spectra are observed in local LIRGs, and high-z IR-bright galaxies (see e.g., Yan et al., 2005, 2007; Dey et al., 2008). All our LIRGs except for NGC 2369 have a nuclear activity class derived from optical spectroscopy (see Table 1); three galaxies have a Seyfert classification, two are classified as *composite,* and the rest have an H II-like classification. To compare with these results, there are a number of mid-IR diagnostics that can be used to test for the presence of an AGN and to determine its contribution to the observed luminosity of the system, as well as to identify highly obscured AGN.

AGN usually show high excitation lines. In the mid-IR the brightest high excitation lines are [Ne V]14.32 μm and [O IV]25.89 μm (e.g., Genzel et al., 1998; Sturm et al., 2002; Meléndez et al., 2008). The large excitation potentials of the [Ne V]14.32 μm and the [O IV]25.89 μm lines (97.1 and 54.9 eV, respectively, see Alexander et al., 1999) make it unlikely that they are excited by star-formation. Moreover, the [O IV]25.89 μm line appears to be a good tracer of the AGN intrinsic luminosity (Meléndez et al., 2008; Diamond-Stanic et al., 2009; Rigby et al., 2009). We note however that these high excitation emission lines are not always detected in relatively bright AGN (e.g., Weedman et al., 2005). IR-bright LINERs also show the [O IV]25.89 μm emission line, but their mid-IR spectral energy distributions are more similar to those of starburst galaxies (Sturm et al., 2006). Moreover, faint extended [O IV]25.89 μm line emission has been detected in some starburst galaxies, indicating that it can also be associated with star formation (Lutz et al., 1998).

Fig. 3 (upper panel) shows the SH nuclear spectra of the three nuclei in our sample classified as Seyfert. The [Ne V]14.32 μm emission line is not detected in Arp 299-B1 (nuclear region of NGC 3690), and the upper limit is consistent with that measured by Verma et al. (2003). In both NGC 5135 and NGC 7130 the [Ne V]14.32 μm line is clearly detected. This may be explained in terms of the lower bolometric luminosity of the AGN in Arp 299-B1 when compared to the AGNs in NGC 5135 and NGC 7130 (Levenson et al., 2004, 2005), *as the [Ne V]14.32 μm appears to be a good indicator of the AGN bolometric luminosity (Dasyra et al., 2008).* The [Ne V]14.32 μm line was not detected in any of the two *composite* nuclei.

The [O IV]25.89 μm line is detected in all the Seyfert nuclei in our sample. In the case of *composite nuclei* (Fig. 3, lower panel), the [O IV]25.89 μm emission line is very faint in NGC 7591, but it is clearly detected in NGC 6701. The latter galaxy contains a large number of bright

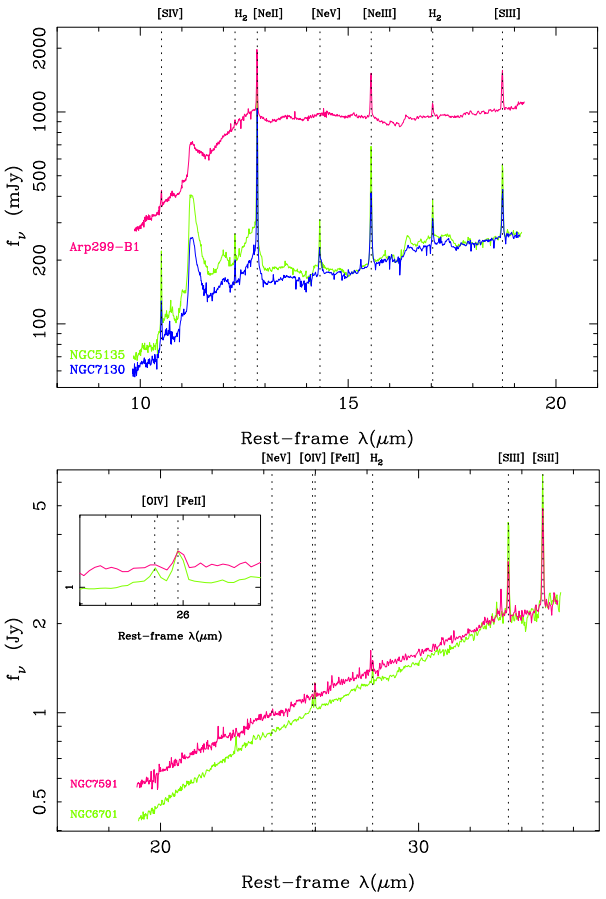

Fig. 3. *Upper panel:* Rest-frame SH spectra of the three nuclei in our sample classified as Seyfert galaxies. The spectra were extracted with square apertures of 4.5 arcsec × 4.5 arcsec in size. The [Ne *v*]14.32 μm emission line is clearly detected in NGC 5135 and NGC 7130, but not in Arp 299-B1. *Lower panel:* Rest-frame LH spectra of the two nuclei in our sample classified as *composite (intermediate between LINER and* H II*) from optical spectroscopy (*Alonso-Herrero et al., 2009b*)*. The spectra were extracted with square apertures of 8.9 arcsec × 8.9 arcsec in size. The [O *iv*]25.89 μm emission line is clearly detected in NGC 6701, but it is very faint in the nuclear region of NGC 7591 (see inset). We also mark in the two panels the positions of other bright mid-IR fine structure lines, *as well as molecular hydrogen lines*.

H II regions within the central (∼ 8.9 arcsec × 8.9 arcsec, the LH extraction aperture) nuclear region (see Alonso-Herrero et al., 2006a, 2009b), and the observed [Ne II]12.82 μm/[O IV]25.89 μm line ratio (∼ 30) is similar to, *although slightly lower than,* those observed in star-forming galaxies in our sample (Pereira-Santaella et al., 2009b). Thus, it is not clear what fraction, if any, of the observed [O IV]25.89 μm line emission is produced by the active nucleus in this galaxy. The possibility that faint [O IV]25.89 μm line emission can also be produced by intense on-going star formation is further confirmed because this line is detected in all the nuclei in our sample classified as H II from optical spectroscopy (see Pereira-Santaella et al., 2009b). Indeed, for the H II-like nuclei in our sample of LIRGs, we measured line ratios of [Ne II]12.82 μm/[O IV]25.89 μm ≫ 10, which are well explained by star formation (see e.g., Genzel et al., 1998; Dale et al., 2006).

An alternative way to identify AGN is to use diagnostic diagrams such as that of the equivalent width (EW) of the 6.2 μm PAH feature[2] feature versus the apparent depth of the 9.7 μm silicate feature put forward by Spoon et al. (2007). Fig. 2 shows such a diagram for the nuclear regions of our sample of LIRGs. For the distances of our galaxies the SL extraction apertures probe regions with physical sizes of between 0.6 and 1.4 kpc, depending on the galaxy. The three Seyfert nuclei in our sample (Arp 299-B1, NGC 5135, and NGC 7130) are located in the 2B region of this diagram, between the region occupied by AGN and that occupied by starburst galaxies, that is, the regions 1A and 1C, respectively (see Spoon et al., 2007 for details). This is in agreement with previous results showing the composite (AGN + star formation) nature of these nuclear regions (see González-Delgado et al., 1998; García-Marín et al., 2006; Alonso-Herrero et al., 2006a,b, 2009; Bedregal et al., 2009 and references therein). Note also the 11.3 μm PAH feature in their nuclear spectra (see Fig. 3, upper panel), clearly indicating the presence of star formation.

The majority of the nuclei in our sample classified as H II or *composite* are located in the 1C starburst region, while only a few nuclear regions (i.e., NGC 2369, Arp 299-A, NGC 3256(S), Zw049.057, and NGC 7591) lie in one of the regions occupied by ULIRGs (the 2B region, see Fig. 2). There are no examples in our sample of LIRG nuclei with very deep silicate features ($S_{Si} < -2.5$) and low EW (< 0.07 μm) of the 6.2 μm PAH feature, that is, the 3A region also occupied by ULIRGs (Spoon et al., 2007).

We can use a diagnostic method similar to that of Nardini et al. (2008) to quantify the relative strengths of AGN and starbursts in nuclei with both. This method is based on the close similarity of the rest-frame 5 − 8 μm spectra of the high (*approximately solar or supersolar, see* Bernard-Salas et al., 2009) metallicity low-*z* starbursts observed by Brandl et al. (2006). Thus, any excess in the 5 − 8 μm spectral region can be attributed to continuum emission from hot dust. Nardini et al. (2008) interpreted this hot dust component as an indication for the presence of an AGN. For our estimate we used two different templates, the starburst template of Brandl et al. (2006) and the star-forming ULIRG template of Nardini et al. (2008). Fig. 4 shows an example of this method applied to source B1 in Arp 299, the nuclear region of NGC 3690. While we did not detect the high excitation [Ne v]14.32 μm line in this nucleus, the AGN is clearly identified via the presence of a strong dust component. This strong dust component is even detected at shorter wavelengths 2–3 μm (see Alonso-Herrero et al., 2000; Soifer et al., 2001). We estimated that the AGN in Arp 299-B1 accounts for ∼ 80–90% of the observed

[2] We measured the EW of the 6.2 μm PAH feature by fitting the local continuum between 5.75 and 6.70 μm and integrating the feature between 5.9 and 6.5 μm. We calculated the EW by dividing the PAH flux by the fitted local continuum at 6.2 μm.

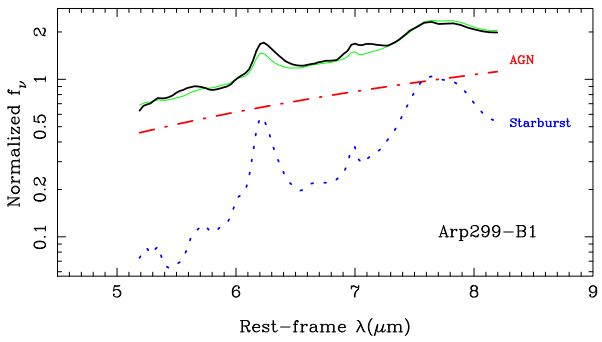

Fig. 4. Rest-frame 5–8 μm spectrum (thick black line) of Arp 299-B1 (see Fig. 1) observed with the SL1 module and extracted with a 3.7 arcsec × 3.7 arcsec aperture. The observed spectrum is normalized at 6 μm. The observed spectrum is modeled (thin green line) as the sum of two components: an AGN continuum (dotted-dashed red line), and a starburst component (dotted blue line) using the Brandl et al. (2006) template. This method is similar to that of Nardini et al. (2008). This figure has been adapted from a similar figure presented by Alonso-Herrero et al. (2009). (For interpretation of color mentioned in this figure legend the reader is referred to the web version of the article.)

emission at 6 μm (see Alonso-Herrero et al., 2009) within a 3.7 arcsec × 3.7 arcsec aperture.

4.2. Star formation properties

4.2.1. Fine structure emission lines

Mid-IR fine structure emission lines can be used to probe the star formation processes in galaxies, with the added advantage that they are less affected by extinction than optical (e.g., Hα) and near-IR (e.g., Paα, Brγ) emission lines. In particular, the [Ne II]12.81 μm line (Roche et al., 1991; Díaz-Santos et al., 2008b), or *alternatively the sum of the [Ne II]*12.81 μm *and the [Ne III]*15.56 μm *emission lines, for very young stellar populations,* appear to be good tracers of the ionizing stars (Ho and Keto, 2007 and references therein). Moreover, because the [Ne III]15.56 μm/[Ne II]12.81 μm line ratio is sensitive to the hardness of the radiation field, it can be used as an indicator of the age of the stellar population. We note however, that this ratio also depends on the metallicity, nebular density and ionization parameter (see e.g., Thornley et al., 2000; Martín-Hernández et al., 2002; Rigby and Rieke, 2004; Snijders et al., 2007).

We find that in general the brightest mid-IR emission lines, [Ne II]12.81 μm, [Ne III]15.56 μm, and [S III]18.71 μm, have an overall morphology similar to that of Hα and Paα (see Alonso-Herrero et al., 2009 and Pereira-Santaella et al., 2009a). Fig. 5 shows an example for one of the LIRGs in our sample: NGC 3110. There is [Ne II]12.81 μm line emission arising from the nuclear region as well as in H II regions as traced by regions of high surface brightness Hα emission in the spiral arms. As found by Alonso-Herrero et al. (2009) for Arp 299, the [Ne III]15.56 μm line emission of NGC 3110 seems to have a better morphological correspondence with the hydrogen recombination line emission (e.g., the H II regions west and south of the nucleus). Another fundamental difference is that the [Ne II]12.81 μm emission line is dominated by the nuclear emission, while the Hα map shows that the nucleus and extra-nuclear regions have a similar brightnesses. This indicates that the Hα nuclear emission is suffering from significant extinction in the optical. The observed apparent depth ($S_{Si} = -0.45$, see Fig. 2) of the 9.7 μm feature implies $A_V \sim 7$ mag, while the extinction derived from optical and near-IR hydrogen recombination lines is $A_V \sim 3$ mag (Veilleux et al., 1995; Alonso-Herrero et al., 2006a).

We also show in Fig. 5 the SH map of the observed [Ne III]15.56 μm/[Ne II]12.81 μm line ratio for NGC 3110. This ratio ranges from 0.1 to approximately 0.4 for NGC 3110, which is similar to the range observed in the majority of the star-forming LIRGs (∼ 0.1–0.8) in our sample (see Pereira-Santaella et al., 2009a) and other high-metallicity starburst galaxies (see Thornley et al., 2000; Verma et al., 2003; Brandl et al., 2006). In our *non-AGN* LIRGs, the lowest values of this ratio are generally coincident with the nuclear regions, whereas the largest values are associated with extra-nuclear H II regions and regions of diffuse low surface brightness Hα or Paα emission (see Fig. 5, and also Alonso-Herrero et al., 2009). The relatively low values of this ratio in most of the nuclear regions of LIRGs could be explained in terms of density effects, as for a given age the ratio decreases for increasing densities; the effect is most noticeable at high densities[3] ($n_H > 10^4$ cm^{-3}, see Snijders et al., 2007). Other effects include the presence of relatively evolved starbursts (see discussions by Thornley et al., 2000 and Alonso-Herrero et al., 2009) and metallicity effects (see Verma et al., 2003; Snijders et al., 2007). Alternatively, the youngest stars may still be embedded in ultra-compact H II regions where the extinction is very high and the ionized gas is at densities exceeding the critical densities of the neon lines (see Rigby and Rieke, 2004).

Higher [Ne III]15.56 μm/[Ne II]12.81 μm line ratios are seen at increasing galactocentric distances and in regions of diffuse ionized gas in LIRGs (see Alonso-Herrero et al., 2009 for Arp 299), and also in other galaxies: NGC 253 (Devost et al., 2004), M82 (Beirão et al., 2008), and NGC 891 (Rand et al., 2008). These high ratios may also be related to the mechanisms responsible for the increased optical line ratios (e.g., [S II]λλ6716,6731/Hα, see a review by Haffner et al., 2009) in regions of diffuse emission, although current models are not able to reproduce the observed [Ne III]15.56 μm/[Ne II]12.81 μm line ratios (see Binette et al., 2009).

4.2.2. PAH feature emission

The mid-IR spectral range contains a large number of PAH features, with the most prominent ones being at 6.2, 7.7, 8.6 and 11.3 μm. High metallicity star forming galaxies

[3] The critical densities are 1.8×10^5 cm^{-3} and 6.1×10^5 cm^{-3} for [Ne III]15.56 μm and [Ne II]12.81 μm, respectively.

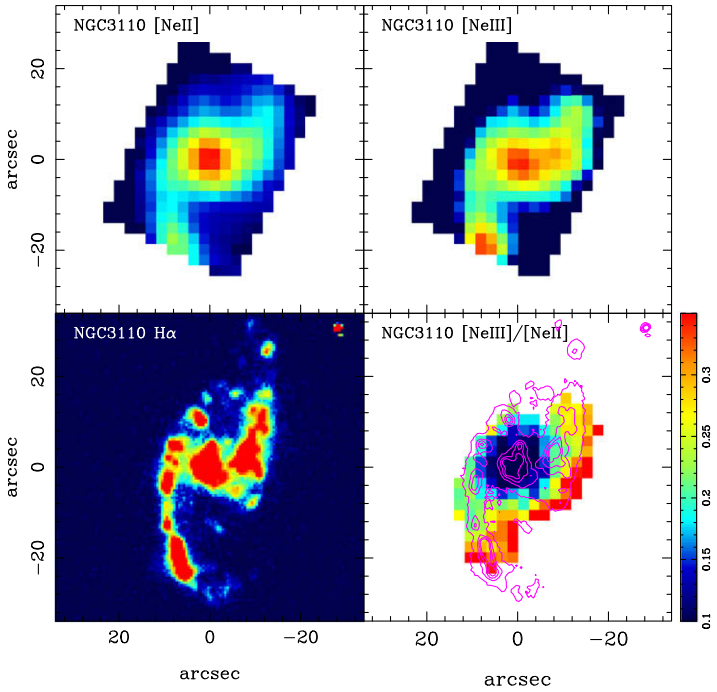

Fig. 5. The upper panels are the observed IRS SH spectral maps of the [Ne *ii*]12.81 μm (left) and [Ne *iii*]15.56 μm (right) emission lines, both displayed in a square root scale. *For these two emission line maps, we only plot pixels with line peak detections* $\geqslant 1\sigma$ *above the continuum, where* σ *is the standard deviation of the continuum fit.* The lower left panel is the continuum-subtracted Hα map of NGC 3110 from Hattori et al. (2004) shown in a square root scale. The lower right panel is the SH observed (not corrected for extinction) map of the [Ne *iii*]15.56 μm/[Ne *ii*]12.81 μm line ratio, with the Hα contours (in a linear scale) superimposed. *Only pixels with line peak* $\geqslant 3\sigma$ *detections in both emission lines are used to construct line ratio map.* The IRS maps have been rotated so the orientation is north up, east to the left.

are known to show bright PAH features, while the PAH emission is faint in low-metallicity galaxies (see e.g., Roche et al., 1991; Madden et al., 2006; Engelbracht et al., 2005; Smith et al., 2007a; **?**; Calzetti et al., 2007). The good correlation between the integrated PAH emission and the IR luminosity of high metallicity star-forming galaxies and ULIRGs indicates that the PAH emission is tracing the star formation activity at least on large scales (Brandl et al., 2006; Smith et al., 2007a; Farrah et al., 2007).

All the LIRGs in our sample show bright 6.2 and 11.3 μm PAH emission over the field of view mapped with the IRS. The overall morphologies of the PAH maps are similar to those of the mid-IR fine structure lines and hydrogen recombination lines (see Figs. 5 and 6), although we are limited by the physical scales of a few kpc probed by the IRS spectral mapping observations. This indicates that, at least to first order, the PAH features are tracing the star formation activity of LIRGs. Indeed, Peeters et al. (2004) showed that although PAHs may trace B stars better than O stars, the integrated PAH emission of galaxies appears to be a good overall tracer of the star formation rate. On smaller scales (tens-hundreds of parsecs), however, PAH emission can stem from sites with no evidence for *on-going* massive star formation (Tacconi-Garman et al., 2005; Díaz-Santos et al., 2008b).

Theoretical models predict that the relative strengths of the different PAH features depend on the properties of the dust grains and the charging conditions, as well as the star-light intensity (Draine and Li., 2001). In particular, neutral PAHs are expected to show large 11.3–6.2 μm ratios, whereas ionized PAHs have smaller ratios. The spatially resolved maps of the 11.3 μm/6.2 μm PAH ratio show variations within galaxies on scales of a few kiloparsecs. In some galaxies these variations in the observed PAH ratios can be readily attributed to the effects of the extinction (see also Rigopoulou et al., 1999; Brandl et al., 2006; Beirão

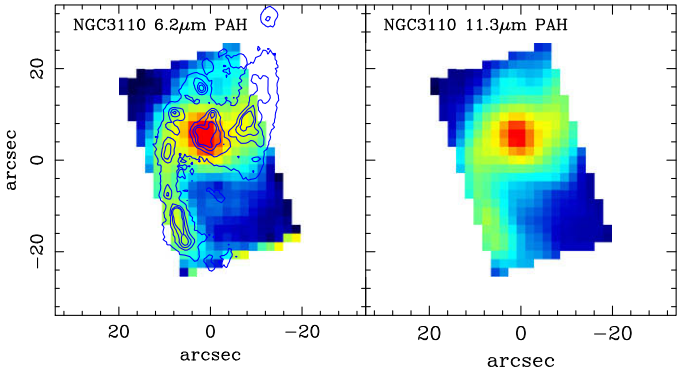

Fig. 6. IRS SL observed (not corrected for extinction) spectral maps of the 6.2 μm (left) and the 11.3 μm PAH features in NGC 3110, shown in a square root scale. The contours are the Hα emission as in Fig. 5. *For both maps, we only plot pixels above* 1σ. The IRS maps have been rotated so the orientation is north up, east to the left.

et al., 2008), as is the case for Arp 299-A (see Alonso-Herrero et al., 2009 and Fig. 1) and other galaxies in the sample. We find however, that in other LIRGs there is no correlation between the observed 11.3 μm/6.2 μm PAH ratio and the apparent depth of the 9.7 μm silicate feature, and it is possible that the variations of this ratio may be showing variations in the physical conditions within galaxies, and from galaxy to galaxy. In a forthcoming paper, Pereira-Santaella et al. (2009a), we will discuss fully this subject for our sample of LIRGs.

5. Integrated mid-IR spectra of LIRGs

Since the IRS maps cover all or nearly all of the mid-IR emitting regions in these galaxies, we combined the full SL + LL data cubes into single mid-IR spectra for each galaxy. We show a few examples covering the full range of IR luminosities of the integrated mid-IR spectra in our sample in Fig. 7, as an illustration of the variety of spectral shapes. The spectra have been normalized at 30 μm for an easy comparison with the typical mid-IR spectra of ULIRGs presented by Armus et al. (2007, their Fig. 2, lower panel). It is clear from Fig. 7 that the integrated spectra of the majority of LIRGs do not show the deep silicate features characteristic of ULIRGs (see also Fig. 2), and are quite similar to the mid-IR spectra of local starburst galaxies (Fig. 8). It is also apparent that there is no clear relation between the IR luminosity and the apparent depth of the silicate feature. For instance, the integrated spectrum of Zw 049.57 shows the deepest silicate feature, whereas the most luminous system in our sample, Arp 299, has an apparent depth of the silicate feature of $S_{Si} \sim -0.8$ (compare with the apparent depth of Arp 299-A, see Fig. 1).

In what follows, we describe a few examples of the potential applications of these kinds of templates.

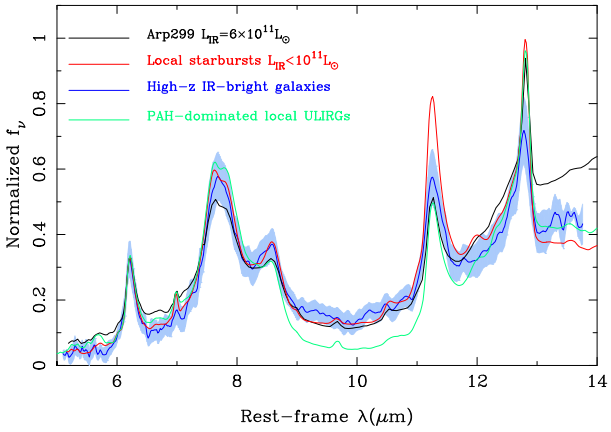

Fig. 8. Comparison of the low spectral-resolution SL spectra of the integrated emission of Arp 299 (*black line*) with the average template *of local starbursts (red line*) of Brandl et al. (2006), the average spectrum of PAH-dominated local ULIRGs (the 2C class of Spoon et al., 2007, see also Fig. 2, *green line*), and the average spectrum and corresponding 1σ dispersion of high-z IR-bright galaxies (*blue line and shaded blue area*) from the Farrah et al. (2008) sample. The IR (1–1000 μm) luminosity range of the galaxies included in this high-z template is $\sim 8\times10^{12}$ to 6×10^{13} $L_{\odot}$. The spectra have been scaled to match the peak of the 6.2 μm PAH feature. This figure has been adapted from Alonso-Herrero et al. (2009). (For interpretation of color mentioned in this figure legend the reader is referred to the web version of the article.)

5.1. Comparison with IR-bright galaxies at high-z

One of the most surprising results obtained with very sensitive *IRS* observations is that a large fraction of IR-selected galaxies at high-z are classified as ULIRGs in terms of their IR luminosities, but their mid-IR spectra are more similar to those of local star-forming galaxies (e.g., Yan et al., 2007; Farrah et al., 2008; Rigby et al., 2008). Specifically, high-z ULIRGs show strong PAH features and moderate depths of the 9.7 μm silicate feature, while their local counterparts tend to show very deep silicate features and moderate to low equivalent widths of

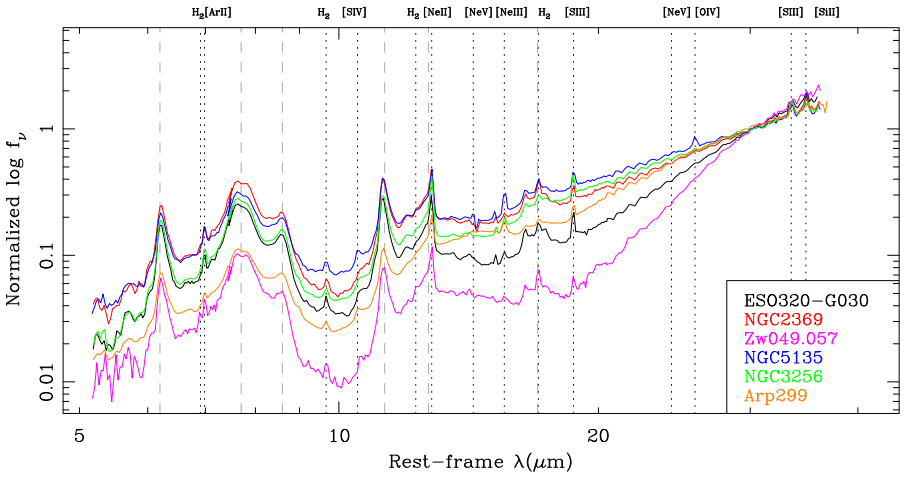

Fig. 7. Integrated low resolution (matched SL + LL) 1D spectra of six LIRGs in our sample spanning the full range of IR luminosity and normalized at 30 μm. We mark the positions of the brightest mid-IR emission lines (dotted lines), as well as the 6.2 and 8.6 μm PAH features and the 7.7, 11.3, 12.7 μm, and 17 μm PAH complexes (dashed lines).

the PAHs (e.g., Spoon et al., 2007; Armus et al., 2007; Farrah et al., 2007).

In Alonso-Herrero et al. (2009) we showed that the integrated spectrum of one of the galaxies in our sample: Arp 299, and the average spectrum of the Farrah et al. (2008) high-z ULIRGs are remarkably similar (see Fig. 8). One of the favored explanations for the observed mid-IR spectra of high-z ULIRGs is that star formation is diffuse and extended, or distributed in multiple dusty star-forming regions spread over several kiloparsecs (Farrah et al., 2008; Rigby et al., 2008). A similar behavior is found for the mid-IR spectra of submillimeter galaxies, which are again interpreted as arising from regions with sizes of a few kiloparsecs (see Menéndez-Delmestre et al., 2009). This is reminiscent of Arp 299, where the star formation is spread across at least 6–8 kpc (see Soifer et al., 2001; Gallais et al., 2004; Alonso-Herrero et al., 2009), with a large fraction taking place in regions of moderate mid-IR optical depths (Fig. 1, upper panel). The majority of the local LIRGs in the representative sample of Alonso-Herrero et al. (2006a) behave in this manner, that is, the mid-IR emission is more extended (a few kpc, Alonso-Herrero et al., 2006b; Díaz-Santos et al., 2008a) than the highly embedded nuclear regions on sub-kiloparsec scales typical of local ULIRGs (Soifer et al., 2000). In *Arp 299, it* is only the nuclear region of IC 694 (Arp 299-A) that shows some of the typical mid-IR characteristics of ULIRGs (see Fig. 2), that is, very compact and embedded star formation resulting in a deep silicate feature and moderate EW of the PAHs. Arp 299 then may be a local counterpart of the star formation processes taking place in high-z IR-bright galaxies (see also Charmandaris et al., 2004), albeit with a lower IR luminosity and possibly higher metallicity.

5.2. Star formation rates for IR galaxies

Observations at 24 μm with the Multiband Imaging Photometer for *Spitzer* (MIPS, Rieke et al., 2004) have proven to be extremely successful in identifying high-z IR bright galaxies. One of the main problems faced by these high-z studies is to determine accurate SFRs for dusty galaxies where UV and optical SFR indicators can be severely affected by extinction effects. Moreover, because of the variety of spectral energy distributions (SEDs) of these IR bright galaxies, and the current lack of sensitive observations at $\lambda > 24$ μm, one has to make assumptions about the IR SEDs (e.g., use theoretical templates) to convert the observed monochromatic IR luminosities into total IR luminosities.

In a recent paper, Rieke et al. (2009), we used the observed mid-IR spectra of some of the local LIRGs discussed here, as well as of starburst galaxies (from Brandl et al., 2006) and ULIRGs (from Rigopoulou et al., 1999 and Armus et al., 2007), together with UV, optical and near-IR photometry to construct average templates covering the range in IR luminosities of $9.75 \leqslant \log L_{\rm IR}(L_{\odot}) \leqslant 13$. The main criteria for the selected galaxies were that: (1) they have good high quality data covering the full electromagnetic spectrum, from the UV to submillimeter wavelengths, and (2) they are only powered by star formation. These templates were then used to determine the relation between the observed mid-IR flux density and the SFR as a function of the redshift of the galaxy. These predictions were computed for a number of different mid and far-IR filters, with wavelengths between 18 and 100 μm, of MIPS on *Spitzer*, PACS (Poglitsch et al., 2008) on *Herschel*, and MIRI (Wright et al., 2004) on the James Webb Space Telescope (*JWST*). We refer the reader to Rieke et al. (2009) for full details.

5.3. Prospects for future space IR missions

Another interesting application of the integrated mid-IR spectra of local LIRGs is to make predictions for future mid and far-IR missions of the detectability of bright mid-IR fine structure emission lines for high-z LIRGs, again to take advantage of the reduced extinction for these dusty objects. This is of particular interest because a large fraction of high-z IR-selected galaxies, submillimeter galaxies and massive galaxies as well as active galaxies appear to be powered by both AGN and star formation activity (e.g., Polletta et al., 2006; Yan et al., 2007; Daddi et al., 2007; Pope et al., 2008a,b; Dey et al., 2008; Alonso-Herrero et al., 2008; Ramos Almeida et al., 2009). Since so far these results have been mostly based on the observed SEDs and/or low spectral resolution IRS spectroscopy, disentangling the AGN and star formation contributions can be challenging. Future IR missions will have the sensitivity and spectral resolution to detect mid-IR emission lines from high-z galaxies. As an illustration, we have simulated their detectability for three IR instruments using the current predicted sensitivities: PACS (Poglitsch et al., 2008) on *Herschel*, MIRI (Gillian Wright, 2009, private communication) on the *JWST*, and SPICA (Swinyard et al., 2009).

We have chosen three LIRGs in our sample to cover a range of IR luminosities as well as different mechanisms contributing to the IR emission. Arp 299 has an IR luminosity close to the ULIRG limit and contains regions of intense star formation as well as at least one low-luminosity ($L_{2-10\rm keV} = 1.1 \times 10^{41}$ erg s^{-1}, Ballo et al., 2004) obscured AGN. NGC 7130 has an intermediate IR luminosity and hosts a Compton-thick AGN (observed luminosity $L_{2-10\rm keV} = 8.9 \times 10^{40}$ erg s^{-1} and estimated intrinsic AGN luminosity $L_{2-10\rm keV} \sim 10^{43}$ erg s^{-1}, Levenson et al., 2005) and star formation in the nuclear region and spread throughout the galaxy. IC 5179 is a moderately luminous IR system and appears to be only powered by star formation. For all these three galaxies we measured the fluxes of the brightest fine structure emission lines from the integrated SH and LH spectra (see Pereira-Santaella et al., 2009a,b). We computed the Brα fluxes from the extinction-corrected Paα fluxes *reported by* Alonso-Herrero et al. (2006a), assuming case B recombination. These fluxes

were measured over regions with sizes similar to those mapped with the IRS.

In Fig. 9 we present the results for the detectability (5σ, 1 h integration time) of the brightest mid-IR emission lines of LIRGs as a function of redshift and the three IR instruments. The simulations assumed that the line emission is unresolved, and thus, for the majority of the lines the detectability is an upper limit as the line emission is expected to be extended in most cases. The tracers of star formation (i.e., Brα, [Ne II]12.81 μm and [Ne III]15.56 μm) in LIRGs will be detected with MIRI and SPICA out to redshift of $z \sim 1$. These lines have the advantage of both a reduced extinction and a relatively straightforward interpretation in terms of the current SFR. The [Ne V]14.31 μm line, which provides definite evidence for the presence of an AGN, will be detected out to $z \sim 0.5$ with MIRI and SPICA for Compton-thick AGN hosted by LIRGs and

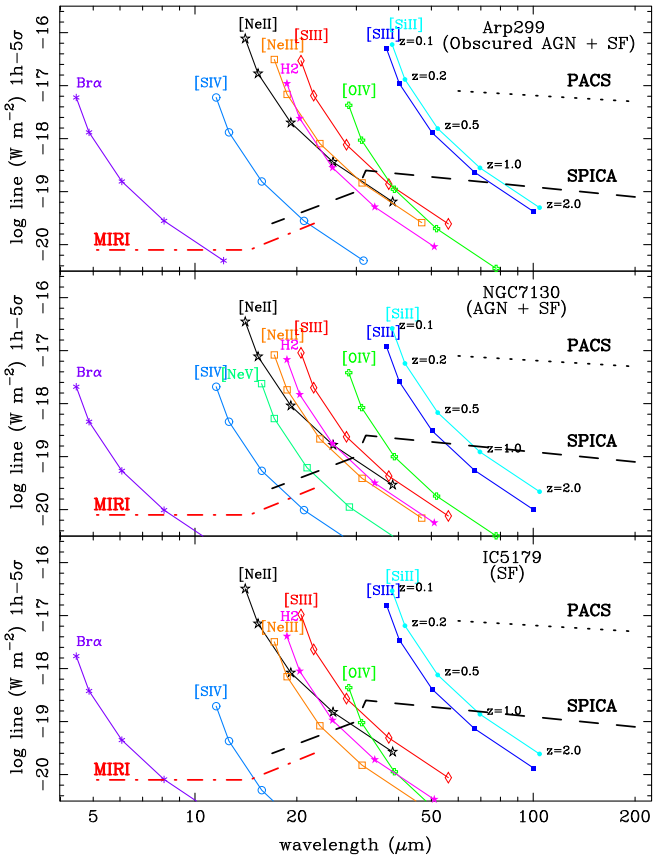

Fig. 9. Predictions as a function of redshift of the detectability (5σ) of Brα, bright mid-IR fine structure lines and the brightest molecular hydrogen line (H_2 S(1)) in LIRGs for future IR missions for 1 h integration time. The predicted sensitivity curves are from Wright et al. (2008) for *JWST*/MIRI (dotted-dashed line), from Swinyard et al. (2009) for SPICA (dashed line) and from Poglitsch et al. (2008) for *Herschel*/PACS (dotted line). We simulated the following emission lines: Brα at 4.05 μm, [S IV]10.51 μm, [Ne II]12.81 μm, [Ne V]14.32 μm, [Ne III]15.56 μm, H_2 S(1) at 17 μm, [S III]18.71 μm, [O IV]25.89 μm, [S III]33.48 μm, and [Si II]34.82 μm. We assumed $H_0 = 71$ km s^{-1} Mpc^{-1}, $\Omega_M = 0.27$, and $\Omega_\Lambda = 0.73$ for these simulations. The simulations are for the integrated line fluxes of three LIRGs in our sample: Arp 299 with $L_{IR} \sim 8 \times 10^{11}$ $L_\odot$, NGC 7130 with $L_{IR} \sim 3 \times 10^{11}$ $L_\odot$, and IC 5179 with $L_{IR} \sim 2 \times 10^{11}$ $L_\odot$.

other types galaxies (e.g., X-ray selected AGN). Finally other bright mid-IR lines such as the [S III]18.71 μm, [S III]33.48 μm, and [Si II]34.82 μm lines and the 17 μm H_2 S(1) transition. The latter is a good tracer of the warm molecular gas in the ISM, and will be easily detected out to at least $z \sim 0.5$ with SPICA.

6. Conclusions

We presented a GTO *Spitzer*/IRS program aimed to obtain mid-IR (5–38 μm) spectral mapping of a sample of 14 local LIRGs covering *at least* the central 20 arcsec × 20 arcsec to 30 arcsec × 30 arcsec regions. We used all four IRS modules: SL, LL, SH, and LH. We constructed spectral maps of the bright mid-IR emission lines (e.g., [Ne II]12.81 μm, [Ne III]15.56 μm, [S III]18.71 μm,H_2 at 17 μm), continuum, the 6.2 and 11.3 μm PAH features, and the 9.7 μm silicate feature. The physical scales *resolved* by the short-wavelength module maps (SL and SH) are between ~ 0.7 kpc for the nearest objects to ~ 2 kpc for the most distant LIRGs in our sample. We also extracted 1D spectra of regions of interest in each galaxy. The main goal of this paper is to describe the goals and present the first results of this *Spitzer*/IRS GTO program.

For a large fraction of the LIRGs in our sample, the regions with the deepest 9.7 μm silicate feature are coincident with the nuclei of the galaxies. The nuclear values of the apparent depth of the silicate feature are moderate (*mostly between* $S_{Si} \sim -0.4$ to $S_{Si} \sim -0.9$), and thus are intermediate between the heavily absorbed nuclei of ULIRGs and the relatively shallow silicate features of starburst galaxies. Only three nuclei, Zw 049.057, Arp 299-A and NGC 3256(S), have deep silicate features ($S_{Si} < -1$).

Since all but one nuclei have a nuclear activity classification from optical spectroscopy, we applied a number of diagnostics to test for the presence of an AGN. In particular we looked for the high excitation [Ne V]14.32 μm and [O IV]25.89 μm emission lines and the presence of a strong dust continuum emission at 6 μm. We found that for the three nuclei classified as Seyfert the mid-IR diagnostics gave a consistent classification. We detected [O IV]25.89 μm emission in most of the LIRG nuclei classified as H II-like or *composite (intermediate between LINER and H II)* from optical spectroscopy, as well as in the Seyfert nuclei. We determined, however, that the large observed [Ne II]12.81 μm/[O IV]25.89 μm line ratios ($\gg 10$) of H II-like nuclei are consistent with being produced by star formation processes rather than by an AGN.

The morphologies of [Ne II]12.81 μm, [Ne III]15.56 μm and the PAH features (at 6.2 and 11.3 μm) of LIRGs are similar to those of hydrogen recombination lines, on the scales probed by the IRS data – a few kiloparsecs. This indicates that the integrated [Ne II]+[Ne III] emission, as well as the PAH emission trace well the star formation activity in this kind of galaxies.

We finally used the integrated *Spitzer*/IRS spectra as templates of local LIRGs. We showed that the integrated

spectra of local LIRGs and in particular that of Arp 299, are similar to those of high-z ULIRGs. This adds support to the scenario where star-formation in high-z IR-bright galaxies is spread over several kiloparsecs, rather than in the highly embedded compact (<1 kpc) nuclear regions of local ULIRGs. Among the different applications of these templates, we used them to predict the intensities of the brightest mid-IR emission lines for LIRGs as a function of redshift and compare them with the expected sensitivities of future space IR missions. The brightest mid-IR emission lines of LIRGs will be detected out to $z \sim 1$, and may be used to constrain better the AGN and star-formation properties of IR-bright galaxies.

The authors would like to thank Takashi Hattori, Macarena García-Marín, Bernhard Brandl, Vassilis Charmandaris, Lee Armus, Guido Risaliti, Henrik Spoon, John Moustakas, and Duncan Farrah for their help and enlightening discussions, as well as Miwa Block for producing some of the data cubes. *We are grateful to two anonymous referees for their constructive comments on the paper.*

This work was supported by NASA through Contract 1255094 issued by JPL/California Institute of Technology. A.A.-H., M.P.-S., L.C., and T.D.-S. acknowledge support from the Spanish Plan Nacional del Espacio through Grant ESP2007-65475-C02-01. A.A.-H. also acknowledges support from the Spanish Ministry of Science and Innovation through Grant Proyecto Intramural Especial 200850I003.

This research has made use of the NASA/IPAC Extragalactic Database (NED), which is operated by the Jet Propulsion Laboratory, California Institute of Technology, under contract with the National Aeronautics and Space Administration.

References

Alexander, T., Sturm, E., Lutz, D., Sterberg, A., Netzer, H., Genzel, R. A&A 512, 204–223 , 1999.

Alonso-Herrero, A., Rieke, G.H., Rieke, M.J., Scoville, N.Z. ApJ 532, 845–866, 2000.

Alonso-Herrero, A., Rieke, G.H., Rieke, M.J., Colina, L., Pérez-González, P.G., Ryder, S.D. ApJ 650, 835–849, 2006a.

Alonso-Herrero, A., Colina, L., Packham, C., Díaz-Santos, T., Rieke, G.H., Radomski, J.T., Telesco, C.M. ApJ 652, L83–L87, 2006b.

Alonso-Herrero, A., Pérez-González, P.G., Rieke, G.H., Alexander, D.M., Rigby, J.R., Papovich, C., Donley, J.L., Rigopoulou, D. ApJ 677, 127–136, 2008.

Alonso-Herrero, A., Rieke, G.H., Colina, L., Pereira-Santaella, M., García-Marín, M., Smith, J.-D. T., Brandl, B., Charmandaris, V., Armus, L. ApJ 697, 660–675, 2009a.

Alonso-Herrero, A., García-Marín, M., Monreal-Ibero, A., Colina, L., Arribas, S., Alfonso-Garzón, J., Labiano, A. A&A, astro-ph/0907.5105, in press, 2009b.

Armus, L., Charmandaris, V., Spoon, H.W.W., et al. ApJS 154, 178–183, 2004.

Armus, L., Charmandaris, V., Bernard-Salas, J., et al. ApJ 656, 148–167, 2007.

Armus, L., Mazzarella, J.M., Evans, A.S., et al. PASP, 121, 559–576, 2009.

Ballo, L., Braito, V., Della Ceca, R., et al. ApJ 600, 634–639, 2004.

Bedregal, A.G., Colina, L., Alonso-Herrero, A., Arribas, S. ApJ 698, 1852–1871, 2009.

Beirão, P., Brandl, B.R., Appleton, P.N., et al. ApJ 676, 304–316, 2008.

Bernard-Salas, J., Spoon, H.W.W., Charmandaris, V. ApJ, astro-ph/0908.2812, in press, 2009.

Binette, L., Flores-Fajardo, N., Raga, A.C., Drissen, L., Morisset, C. ApJ 695, 552–560, 2009.

Brandl, B.R., Bernard-Salas, J., Spoon, H.W.W., et al. ApJ 653, 1129–1144, 2006.

Calzetti, D., Kennicutt, R.C., Engelbracht, C.W., et al. ApJ 666, 870–895, 2007.

Caputi, K.I., Lagache, G., Yan, L., et al. ApJ 660, 97–116, 2007.

Charmandaris, V., Le Floc'h, E., Mirabel, I.F. ApJ 600, L15–L18, 2004.

Daddi, E., Alexander, D.M., Dickinson, M., et al. ApJ 670, 173–189, 2007.

Dale, D.A., Smith, J.D.T., Armus, L., et al. ApJ 646, 161–173, 2006.

Dasyra, K., Ho, L.C., Armus, L., Ogle, P., Helou, G., Peterson, B.M., Lutz, D., Netzer, H., Sturm, E. ApJ 674, L9–L12, 2008.

Devost, D., Brandl, B.R., Armus, L., et al. ApJS 154, 242–247, 2004.

Dey, A., Soifer, B.T., Desai, V., et al. ApJ 677, 943–956, 2008.

Diamond-Stanic, A.M., Rieke, G.H., Rigby, J.R. ApJ 698, 623–631, 2009.

Díaz-Santos, T., Alonso-Herrero, A., Colina, L., Packham, C., Radomski, J., Telesco, C.M. ApJ 685, 211–224, 2008a.

Díaz-Santos, T., Alonso-Herrero, A., Colina, L., Packham, C., Levenson, N., Pereira-Santaella, M., Roche, P., Telesco, C.M. ApJ, submitted for publication, 2008b.

Draine, B.T., Li, A. ApJ 551, 807–824, 2001.

Elbaz, D., Cesarsky, C.J., Chanial, P., Aussel, H., Franceschini, A., Fadda, D., Chary, R.R. A&A 384, 848–865, 2002.

Engelbracht, C.W., Gordon, K.D., Rieke, G.H., Werner, M.W., Dale, D.A., Latter, W.B. ApJ 628, L29–L32, 2005.

Farrah, D., Lonsdale, C.J., Weedman, D.W., et al. ApJ 677, 957–969, 2008.

Farrah, D., Bernard-Salas, J., Spoon, H.W.W., et al. ApJ 667, 149–169, 2007.

Gallais, P., Charmandaris, V., Le Floc'h, E., Mirabel, I.F., Sauvage, M., Vigroux, L., Laurent, O. 414, 845–855, 2004.

García-Marín, M., Colina, L., Arribas, S., Alonso-Herrero, A., Mediavilla, E. ApJ 650, 850–871, 2006.

Genzel, R., Lutz, D., Sturm, E., et al. ApJ 498, 579–605, 1998.

González-Delgado, R.M., Heckman, T., Leitherer, C., Meurer, G., Krolik, J., Wilson, A.S., Kinney, A., Koratkar, A. ApJ 505, 174–198, 1998.

Haffner, L.M., Dettmar, R.-J., Beckman, J.E., et al. RvMP 81, 969–997, 2009.

Hao, L., Weedman, D.W., Spoon, H.W.W., Marshall, J.A., Levenson, N.A., Elitzur, M., Houck, J.R. ApJ 655, L77–L80, 2007.

Hattori, T., Yoshida, M., Ohtani, H., Sugai, H., Ishigaki, T., Sasaki, M., Hayashi, T., Ozaki, S., Ishii, M., Kawai, A. AJ 127, 736–757, 2004.

Ho, L., Keto, E. ApJ 658, 314–318, 2007.

Houck, J.R., Roellig, T.L., vanClee, J., et al. ApJS 154, 18–24, 2004.

Kennicutt Jr., R.C. ARA&A 36, 189–232, 1998.

Lagache, G., Puget, J.-L., Dole, H. ARA&A 43, 727–768, 2005.

Le Floc'h, E., Papovich, C., Dole, H., et al. ApJ 632, 169–190, 2005.

Levenson, N.A., Weaver, K.A., Heckman, T.M., Awaki, H., Terashima, Y. ApJ 602, 135–147, 2004.

Levenson, N.A., Weaver, K.A., Heckman, T.M., Awaki, H., Terashima, Y. ApJ 618, 167–177, 2005.

Levenson, N.A., Sirocky, M.M., Hao, L., Spoon, H.W.W., Marshall, J.A., Elitzur, M., Houck, J.R. ApJ 645, L45–L48, 2007.

Lutz, D., Kunze, D., Spoon, H.W.W., Thornley, M.D. A&A 333, L75–L78, 1998.

Madden, S.C., Galliano, F., Jones, A.P., Sauvage, M. A&A 446, 877–896, 2006.

Martín-Hernández, N.L., Peeters, E., Morisset, C., et al. A&A 381, 606–627, 2002.

Meléndez, M., Kraemer, S.B., Armentrout, B.K., et al. ApJ 682, 94–103, 2008.

Menéndez-Delmestre, K., Blain, A.W., Smail, I., Alexander, D.M., Chapman, S.C., Armus, L., Frayer, D., Ivison, R.J., Teplitz, H. ApJ 699, 667–685, 2009.
Murphy Jr., T.W., Soifer, B.T., Matthews, K., Armus, L. ApJ 559, 201–224, 2001.
Nardini, E., Risaliti, G., Salvati, M., Sani, E., Imanishi, M., Marconi, A., Maiolino, R. MNRAS 385, L130–L134, 2008.
Peeters, E., Spoon, H.W.W., Tielens, A.G.G.M. ApJ 613, 986–1013, 2004.
Pereira-Santaella, M., Alonso-Herrero, A., Rieke, G.H., Colina, L., Díaz-Santos, T., Pérez-González, P.G., Smith, J.-D.T., Engelbracht, C.W. ApJS, submitted for publication, 2009a.
Pereira-Santaella, M., Alonso-Herrero, A., Rieke, G.H., Colina, L., et al., in preparation, 2009b.
Pérez-González, P.G., Rieke, G.H., Egami, E., et al. ApJ 630, 82–107, 2005.
Poglitsch, A., Waelkens, C., Bauer, O.H., et al. SPIE 7010, 701005, 2008.
Polletta, M.C., Wilkes, B.J., Siana, B., et al. ApJ 642, 673–693, 2006.
Pope, A., Brussmann, R.S., Dey, A., et al. ApJ 689, 127–133, 2008a.
Pope, A., Chary, R.-R., Alexander, D.M., et al. ApJ 675, 1171–1193, 2008b.
Ramos Almeida, C., Rodríguez-Espinosa, J.M., Barro, G., Gallego, J., Pérez-González, P.G. AJ 137, 179–196, 2009.
Rand, R.J., Wood, K., Benjamin, R.A. ApJ 680, 263–275, 2008.
Rieke, G.H., Low, F.J. ApJ 176, L95–L100, 1972.
Rieke, G.H., Lebofsky, M.J. ApJ 288, 618–621, 1985.
Rieke, G.H., Young, E.T., Engelbracht, C.W., et al. ApJS 154, 25–29, 2004.
Rieke, G.H., Alonso-Herrero, A., Weiner, B.J., Pérez-González, P.G., Blaylock, M., Donley, J.L., Marcillac, D. ApJ 692, 556–573, 2009.
Rigby, J.R., Rieke, G.H. ApJ 606, 237–257, 2004.
Rigby, J.R., Marcillac, D., Egami, E., et al. ApJ 675, 262–280, 2008.
Rigby, J.R., Diamond-Stanic, A.M., Aniano, G. ApJ 700, 1878–1883, 2009.
Rigopoulou, D., Spoon, H.W.W., Genzel, R., Lutz, D., Moorwood, A.F.M., Tran, Q.D. AJ 118, 2625–2645, 1999.
Roche, P.F., Aitken, D.K., Smith, C.H., Ward, M.J. MNRAS 248, 606–629, 1991.
Roussel, H., Helou, G., Smith, J.D., et al. ApJ 646, 841–857, 2006.
Sanders, D.B., Mirabel, F.I. ARA&A 34, 749, 1996.
Sanders, D.B., Mazzarella, J.M., Kim, D.-C., Surace, J.A., Soifer, B.T. AJ 126, 1607–1664, 2003.
Shi, Y., Rieke, G.H., Hines, D.C., Gorjian, V., Werner, M.W., Cleary, K., Low, F.J., Smith, P.S., Bouwman, J. ApJ 653, 127–136, 2006.
Sirocky, M.M., Levenson, N.A., Elitzur, M., Spoon, H.W.W., Armus, L. ApJ 678, 729–743, 2008.
Smith, J.D.T., Draine, B.T., Dale, D.A., et al. ApJ 656, 770–791, 2007a.
Smith, J.D.T., Armus, L., Dale, D.A., et al. PASP 119, 1133–1144, 2007b.
Snijders, L., Kewley, L.J., van der Werf, P.P. ApJ 669, 269–288, 2007.
Soifer, B.T., Sanders, D.B., Madore, B., et al. ApJ 320, 238–257, 1987.
Soifer, B.T., Neugebauer, G., Matthews, K., et al. AJ 119, 509–523, 2000.
Soifer, B.T., Neugebauer, G., Matthews, K., et al. AJ 122, 1213–1237, 2001.
Spoon, H.W.W., Marshall, J.A., Houck, J.R., et al. ApJ 654, L49–L52, 2007.
Spoon, H.W.W., Keane, J.V., Tielens, A.G.G.M., Lutz, D., Moorwood, A.F.M. A&A 365, L353–L356, 2001.
Spoon, H.W.W., Koornneef, J., Moorwood, A.F.M., Lutz, D., Tielens, A.G.G.M. A&A 357, 898–908, 2000.
Sturm, E., Lutz, D., Verma, A., et al. A&A 393, 821–841, 2002.
Sturm, E., Rupke, D., Contursi, A., et al. ApJ 653, L13–L16, 2006.
Swinyard, B., Nakagawa, T., Merken, P., et al. ExA 23, 193–219, 2009.
Tacconi-Garman, L.E., Sturm, E., Lehnert, M., Lutz, D., Davies, R.I., Moorwood, A.F.M. A&A 432, 91–103, 2005.
Thornley, M.D., Schreiber, N., Lutz, D., et al. ApJ 539, 641–657, 2000.
Tran, Q.D., Lutz, D., Genzel, D., et al. ApJ 552, 527–543, 2001.
Veilleux, S., Kim, D.-C., Sanders, D.B., Mazzarella, J.M., Soifer, B.T. ApJS 98, 171–217, 1995.
Verma, A., Lutz, D., Sturm, E., et al. A&A 403, 829–846, 2003.
Weedman, D.W., Hao, L., Higdon, S.J.U., et al. ApJ 633, 706–716, 2005.
Wright, G.S., Rieke, G.H., Colina, L., et al. SPIE 5487, 653–663, 2004.
Wu, Y., Charmandaris, V., Hao, L., Brandl, B.R., Bernard-Salas, J., Spoon, H.W.W., Houck, J.R. ApJ 639, 157–172, 2007.
Yan, L., Chary, R., Armus, L., et al. ApJ 620, 604–610, 2005.
Yan, L., Sajinna, A., Fadda, D., et al. ApJ 658, 778–793, 2007.